



Contents lists available at ScienceDirect

Journal of Biomechanics

journal homepage: [www.elsevier.com/locate/jbiomech](http://www.elsevier.com/locate/jbiomech)  
[www.JBiomech.com](http://www.JBiomech.com)

# Rapid identification of elastic modulus of the interface tissue on dental implants surfaces using reduced-basis method and a neural network

Khin Zaw<sup>a,\*</sup>, G.R. Liu<sup>a,b</sup>, B. Deng<sup>a</sup>, K.B.C. Tan<sup>c</sup>

<sup>a</sup> Centre for Advanced Computations in Engineering Science, Department of Mechanical Engineering, National University of Singapore, 9 Engineering Drive 1, Singapore 117576, Singapore

<sup>b</sup> Singapore-MIT Alliance (SMA), E4-04-10, 4 Engineering Drive 3, Singapore 117576, Singapore

<sup>c</sup> Department of Restorative Dentistry, Faculty of Dentistry, National university of Singapore, 5 Lower Kent Ridge Road, Singapore 119074, Singapore

## ARTICLE INFO

### Article history:

Accepted 5 December 2008

### Keywords:

Reduced-basis method  
Neural network  
Material characterization  
Fast computation  
Elastic modulus

## ABSTRACT

This paper proposes a rapid inverse analysis approach based on the reduced-basis method (RBM) and neural network (NN) to identify the “unknown” elastic modulus (Young’s modulus) of the interfacial tissue between a dental implant and the surrounding bones. In the present RBM–NN approach, a RBM model is first built to compute displacement responses of dental implant–bone structures subjected to a harmonic loading for a set of “assumed” Young’s moduli. The RBM model is then used to train a NN model that is used for actual inverse analysis in real-time. Actual experimental measurements of displacement responses are fed into the trained NN model to inversely determine the “true” elastic modulus of the interfacial tissue. As an example, a physical model of dental implant–bone structure is built and inverse analysis is conducted to verify the present RBM–NN approach. Based on numerical simulation and actual experiments, it is confirmed that the identified results are very accurate, reliable, and the computational saving is very significant. The present RBM–NN approach is found robust and efficient for inverse material characterizations in noninvasive and/or nondestructive evaluations.

© 2008 Elsevier Ltd. All rights reserved.

## 1. Introduction

Osseointegration is the structural and functional connection between the living bone and dental implant surface (Bränemark et al., 1985; Friberg et al., 1991; Brunski, 1992). In the osseointegration process, conditions of implant–bone interfacial tissues influence significantly adaptive bone remodelling (Cowin, 1986) and material properties of interfacial tissues determine biomechanical responses and stability of implant–bone structures.

Several research works have been carried out to predict bone properties of implant–bone structure with in-vitro or in-vivo studies (Cowin, 2001). Examples are traditional mechanical testing, nanoindentation, imaging procedures or ultrasonic techniques (Cowin, 2001). A technique of resonance frequency analysis (RFA) (Meredith et al., 1996; Sennerby et al., 2005) has also been developed to detect implant stability. However, no precise method has been developed to determine noninvasively the material properties of implant–bone interfacial tissues after dental implant operations due to technical difficulties. It is, however, invaluable to develop a systematic and efficient inverse approach to identify material properties of interfacial tissues. In the area of nondestructive evaluation (NDE), two pieces of very

important techniques have been made available. One is advanced inverse analysis techniques (Liu and Han, 2003) that allow systematic means to identify system parameters from properly designed measurable outputs. Another one is the so-called real-time computation methods that allow rapid computation of the outputs for a set of assumed inputs. These two pieces of techniques are applicable to identify material properties of dental implant systems.

Currently, the finite element method (FEM) is widely employed to evaluate the behavior of an implant–bone structure (Geng et al., 2001; Deng et al., 2008a,b). A FEM analysis is, however, very time-consuming because of the complexity of implant–bone structures demanding a large amount of elements. In an inverse analysis, thousands and even hundreds of thousands of such “forward” analyses may be required. Thus, the total CPU-time for an inverse analysis can be unacceptably long. A fast forward solver is therefore critical in order to avoid very long CPU-time in inverse analyses.

A reduced-basis method (RBM) (<http://augustine.mit.edu>) is a fast computational technique which can solve forward problems rapidly with desired accuracy. RBMs with error estimation were employed to solve different kinds of partial differential equations. The detailed procedures for reduced-basis method for parametrized parabolic partial differential equations can be found in the work of Nguyen (2005); Grepl and Patera (2005). Applications of the reduced-basis method and its rigorous error

\* Corresponding author. Tel.: +65 65164797; fax: +65 67791459.  
E-mail address: [g0402948@nus.edu.sg](mailto:g0402948@nus.edu.sg) (K. Zaw).

estimation can be found in Veroy and Patera (2005), Rozza and Veroy (2007) for Navier–Stokes equation, in Patera and Rønquist (2007) for Boltzmann equation and in Huynh and Patera (2006) for stress intensity factor analysis. Recently, Liu et al. (2008a) developed a SGP\_RBM method, for elasticity problems, based on a smoothed Galerkin projection (Liu, 2008), which can provide an upper bound to the *exact* solution while the original reduced-basis method provides a lower bound to the *exact* solution. The computational efficiency of such a RBM is found significantly higher compared to that of the FEM, and hence has been applied to inverse analyses of complicated engineering systems to reduce computational cost (Liu et al., 2005).

In the NDE for material and structural systems, inverse searching methodologies (Liu and Han, 2003) including direct search algorithm, gradient-based algorithm, genetic algorithms (GAs) and the neural network (NN), are commonly adopted. Applications of the GAs in inverse analyses can be found in work of Han et al. (2002) and Liu et al. (2002a, 2008b). In additions, the NN has found its applications in inverse problems of elastic wave propagation (Sribar, 1994), material characterizations (Huber and Tsakmakis, 1999) of functionally graded material (FGM) (Han and Liu, 2003; Han et al., 2003; Liu et al., 2001a, b, 2002b), material characterizations of implant-bone structure (Deng et al., 2004, 2008c), and optimal design problems (Sumpter and Noid, 1996). From these earlier studies, it is noted that the NN possesses unique computing features for identification of structural parameters which are non-linearly related to dynamic responses of the structure in a complicated manner. A RBM–NN approach in which a RBM model is developed as a “teacher” to train a NN is proposed in order to make use of the high computational efficiency of the RBM and the efficiency of the NN in performing inverse analyses.

A 3D FEM model is firstly constructed for a dental implant-bone system, and a fast RBM model is developed. The RBM model is then used to generate the displacement responses of the dental implant-bone structure to train a NN model. The trained NN model is next applied to inversely identify elastic moduli of interfacial tissues in the dental implant system by feeding with experimental measurements of the actual physical model of the dental implant system.

## 2. Construction of RBM model

### 2.1. Problem statement

A dental implant-bone problem is considered, and a sectional view of the problem is displayed in Fig. 1. The dental implant-bone system consists of four regions of the outermost cortical bone  $\Omega_1$  the cancellous bone  $\Omega_2$  the region of interfacial tissue  $\Omega_3$  and the aluminium rod of dental implant  $\Omega_4$ :  $\Omega = \cup_{i=1}^4 \Omega_i$ . Material properties of each region are listed in Table 1. A harmonic force of angular frequency  $\omega$  is applied to the aluminium rod, and Dirichlet boundary condition is specified in  $\Gamma_D$  as shown in Fig. 1.

The purpose of our work is to identify inversely the elastic Young's modulus  $E$  of the interfacial tissue between the surface of aluminium rod and the cancellous bone from “measured” displacement responses of the dental bone structure to excitation forces of different frequency  $\omega$ . Our analysis procedure consists of two parts: forward analysis and inverse analysis. The forward analysis determines the response of the system to a set of input of system parameter for which we need to build a RBM model. The inverse analysis determines the Young's modulus  $E$  from a given measurement of response of the dental system when it is excited. In the forward analysis, input parameters  $\mu$  for our forward analyses are defined by  $E$  and the frequency  $\omega$ :  $\mu = (E, \omega) \in \mathcal{D}$  where  $\mathcal{D} = [1.0 \times 10^9, 4.5 \times 10^9] \text{ Pa} \times [500, 3500] \text{ Hz} \subset \mathbb{R}^{p=2}$ . Based

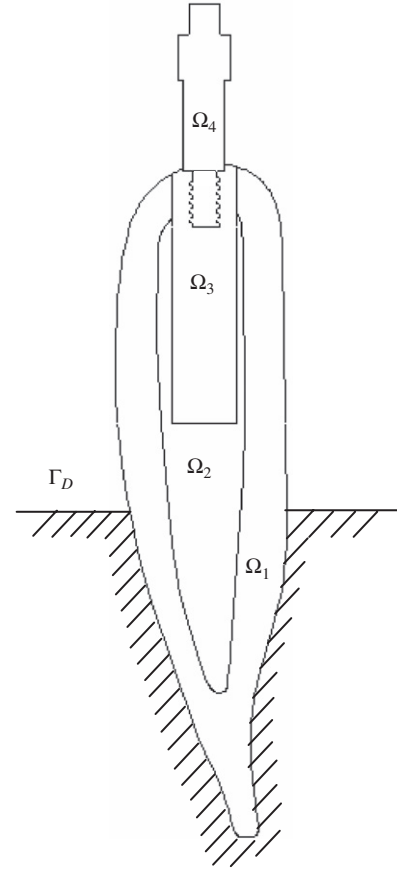


Fig. 1. Diagram of a dental implant-bone structure with four regions.

on the standard weakform of elasticity, for a given  $\mu \in \mathcal{D}$ , the *exact* solution of the *exact* problem satisfies (see, e.g., Grepl et al., 2007; Nguyen, 2005)

$$a(u^e(\mu), v; \mu) = f(v; \mu), \forall v \in \mathbb{S}, \quad (1)$$

where  $\mathbb{S}$  is a proper Hilbert space and the output of interest is determined as

$$s^e(\mu) = \ell(u^e(\mu)), \quad (2)$$

where  $s^e(\mu)$  is the *exact* output,  $u^e(\mu)$  is the *exact* displacement,  $a(\cdot, \cdot)$  is bilinear form and  $\ell$  is linear functional.

The bilinear form  $a(\cdot, \cdot)$  is now transformed into the parametric bilinear form as (Prud'homme et al., 2002)

$$a(w, v; \mu) = \sum_{q=1}^Q \Theta^q(\mu) a^q(w, v), \quad (3)$$

where  $a^q(w, v)$  is  $\mu$ -independent bilinear form and  $\Theta^q(\mu)$  are the coefficient for affine function. This parametric bilinear form is crucial in formulating the reduced-basis method.

#### 2.1.1. Experimental setting

A block of bovine rib of a mature specimen, obtained commercially from a butcher, is used as a physical model for the edentulous human mandible. The experiment procedure strictly abided with the National Advisory Committee for Laboratory Animal Research Guidelines and the General Laboratory Safety Procedure of National University of Singapore.

A  $4 \times 13$  mm implant socket is prepared using drills according to the actual surgery protocol suggested by the manufacturer. To simulate the changes in stiffness of interfacial tissue during the

**Table 1**  
Material properties of dental implant–bone structure.

$\Omega = \cup_{i=1}^4 \Omega_i$	Young modulus: $E$ (Pa)	Poisson Ratio: $\nu$	Density: $\rho$ (g/mm <sup>3</sup> )
Cortical Bone	$2.3162 \times 10^{10}$	0.371	$1.8601 \times 10^{-3}$
Cancellous Bone	$8.2345 \times 10^8$	0.3136	$7.1195 \times 10^{-4}$
Implant–bone interface (resin)	$E$ (variable)	0.3155	$1.055 \times 10^{-3}$
Aluminum rod	$7.05 \times 10^{10}$	0.35	$2.78 \times 10^{-3}$

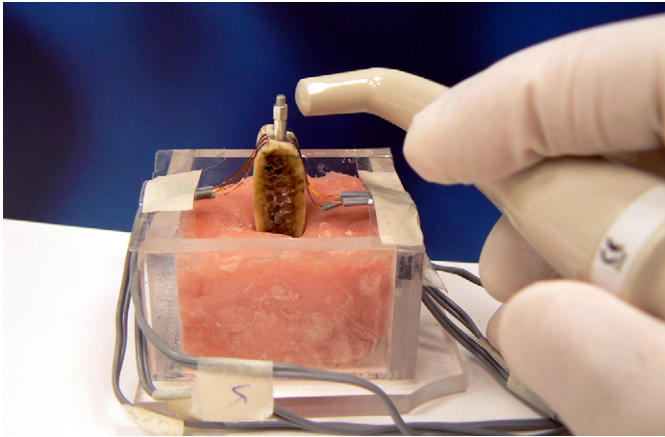


**Fig. 2.** Experimental setting for implant stability measurement.

osseointegration process, the drilled hole is filled with self-curing resin. Instead of using an actual implant, an aluminium rod (SmartPeg™, Osstell AB, Sweden) is inserted in the resin. A RFA device (Osstell Mentor™, Osstell AB, Sweden, [www.osstell.com](http://www.osstell.com)) is used to measure vibration responses of the structure as shown in Fig. 2. The aluminium rod is excited by an electromagnetic pulse from the measurement probe.

### 2.1.2. Finite element approximation

Since it is impossible to obtain the exact solution  $u^e(\mu)$  given in Eq. (1), the FEM solution  $\tilde{u}(\mu)$ , in a discretized space  $\tilde{\mathcal{S}}$  of very large dimension  $\mathfrak{N}$ , is often used in place of  $u^e$ . Based on the FEM theory,  $\tilde{u} \rightarrow u^e$  when  $\tilde{\mathcal{S}} \rightarrow \mathcal{S}$  as  $\mathfrak{N} \rightarrow \infty$  in a proper fashion. A three-dimensional geometry and a 3D FEM model simulating our experimental physical model are then created. The interfaces between the cortical and cancellous bone, interfacial tissue and the bones, interfacial tissue and aluminium rod are assumed to be perfectly bonded. Ten-node tetrahedral elements are used in our FEM model with a total degree of freedom  $\mathfrak{N} = 72,465$  as shown in Fig. 3. For a given parameter  $\mu = (E, \omega) \in \mathcal{D}$ , the FEM seeks the solution  $\tilde{u}$  that satisfies

$$a(\tilde{u}(\mu), v; \mu) = f(v; \mu), \quad \forall v \in \tilde{\mathcal{S}}, \quad (4)$$

where  $a(\tilde{u}(\mu), v; \mu)$  is a parametric bilinear form and  $f(v; \mu)$  is a linear functional. The associated output of interest is defined as

$$\tilde{s}(\mu) = \ell(\tilde{u}(\mu)), \quad (5)$$

where  $\ell$  is a linear functional. The output  $\tilde{s}(\mu)$  is the displacement component in the direction at a position where harmonic force is applied as illustrated in Fig. 3. Therefore, responses of displacement components in that direction are sensitive to the changes of  $E$ , which is very important for our inverse analyses.

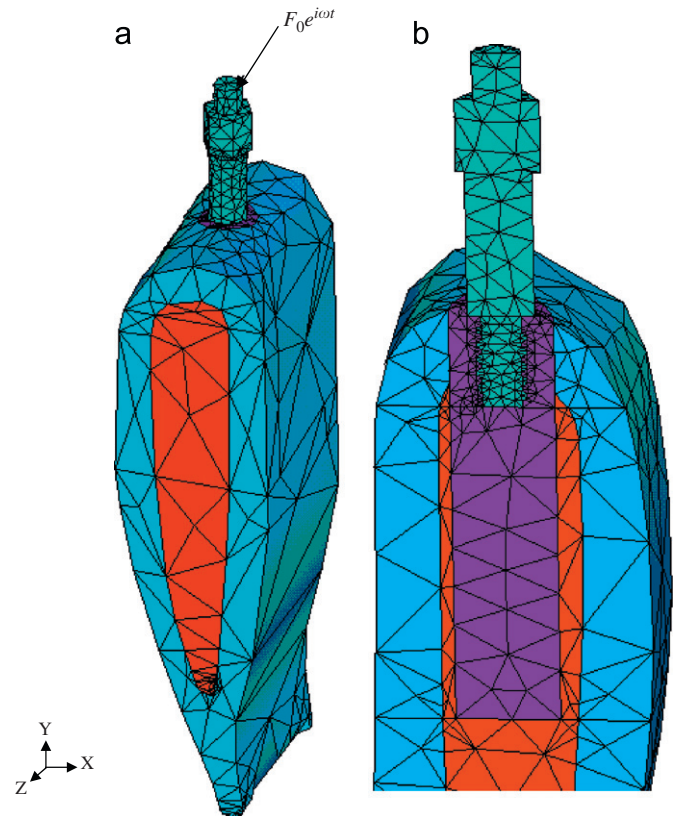


**Fig. 3.** (a) Overall 3-D FEM model of a dental implant–bone structure and (b) sectional view of the interface area.

### 2.2. Reduced-basis method

Since a very fine FEM model is required for  $\tilde{u} \rightarrow u^e$ , it is very expensive to obtain computationally. Therefore, the RBM is chosen to improve the computational efficiency. A reduced-basis sample set in the parameter space  $\mathcal{D}$ ,  $P_N = \{\mu^1 \in \mathcal{D}, \dots, \mu^N \in \mathcal{D}\}$ , where  $\mu \in \mathcal{D} \subset \mathbb{R}^p$  is introduced at the start of the RBM procedure, and the reduced-basis space is defined as  $\tilde{\mathcal{W}}_N = \text{span}\{\zeta^i \equiv \tilde{u}(\mu^i), 1 \leq i \leq N\}$ , where  $\tilde{u}(\mu^i)$  is the FEM solutions for a given  $\mu^i \in P_N$ . For any  $\mu \in \mathcal{D}$ , the RBM approximation  $\tilde{u}_N(\mu)$  satisfies

$$a(\tilde{u}_N(\mu), v; \mu) = f(v; \mu), \quad \forall v \in \tilde{\mathcal{W}}_N, \quad (6)$$

where  $a(\tilde{u}_N(\mu), v; \mu)$  is the parametric bilinear form. The corresponding reduced-basis output of interest can be obtained by

$$\tilde{s}_N(\mu) = \ell(\tilde{u}_N(\mu)). \quad (7)$$

In solving the above equations, the RBM procedure consists of two stages:  $\mu$ -independent offline and  $\mu$ -dependent online stages (Prud'homme et al., 2002). In the offline stage, the  $N$  times of  $\mathfrak{N}$ -dimension FEM analyses are required to create  $\tilde{\mathcal{W}}_N$ . Thus, it is very expensive but it only requires to be done once. In the online stage, the reduced-basis solutions are evaluated very efficiently as

it requires only  $O(N^3)$  operations as  $N \ll \mathfrak{N}$ , where  $N$  and  $\mathfrak{N}$  are the dimension of the RBM model and the FEM model, respectively.

### 2.2.1. Reduced-basis sample construction

Following the procedure given by Liu et al. (2008a, b), the reduced-basis sample set  $P_N$  is now created using asymptotic error estimation and greedy algorithm. Firstly, a sample set  $S^G \subset \mathcal{D}$  is introduced. Reduced-basis sample sets  $P_N = \{\mu^1 \in S^G\}$  and  $P_M = \{\mu^1 \in S^G, \mu^2 \in S^G\}$  are next created, where  $M = 2N$  and  $P_N \subset P_M$ . We set the associated RB spaces  $\tilde{W}_N \subset \tilde{W}_M$  and the desired minimum error tolerance  $\varepsilon_{tol}$ . The asymptotic error is determined as

$$\Delta_{N,M}^s(\mu) = \frac{|\tilde{s}_M(\mu) - \tilde{s}_N(\mu)|}{|\tilde{s}_M(\mu)|}, \quad (8)$$

where  $\tilde{s}_N$  and  $\tilde{s}_M$  are the outputs of  $\tilde{W}_N$  and  $\tilde{W}_M$ . According to the fast convergence of RBM, we anticipate  $\tilde{u}_M \rightarrow \tilde{u}$  and  $\tilde{s}_M \rightarrow \tilde{s}$ . The exact error between  $\tilde{s}_N$  and  $\tilde{s}$  is now defined as

$$\Delta_{N,exact}^s(\mu) = \frac{|\tilde{s}(\mu) - \tilde{s}_N(\mu)|}{|\tilde{s}(\mu)|}. \quad (9)$$

Another parameter set  $S_{test}$  including  $n_{test}$  samples is randomly created in  $\mathcal{D}$ . The averaged asymptotic error and exact error are also defined over  $S_{test} \subset \mathcal{D}$ ,

$$\Delta_{N,M,avg}^s = \frac{\sum_{i=1}^{n_{test}} \Delta_{N,M}^s(\mu_{test}^i \in S_{test})}{n_{test}} \quad \text{and}$$

$$\Delta_{N,exact,avg}^s = \frac{\sum_{i=1}^{n_{test}} \Delta_{N,exact}^s(\mu_{test}^i \in S_{test})}{n_{test}}. \quad (10)$$

Note that the exact error and the averaged errors are used to verify the accuracy of our asymptotic error estimate. Using the asymptotic error, the greedy algorithm is carried out until it found  $\max_{\mu \in S^G} \Delta_{N,M}^s(\mu) \leq \varepsilon_{tol}$  to obtain  $P_N = \{\mu^i \in \mathcal{D}\}$ ,  $i = 1, \dots, N$ .

### 2.3. Numerical results

A sample set  $S^G$  is created in a regular  $31 \times 31$  grid pattern over  $\mathcal{D}$ , and the desired minimum error tolerance is set as  $\varepsilon_{tol} = 10^{-4}$ . The greedy adaptive procedure is carried out to create an optimal RB set  $P_N$  at an optimal  $N_{max} = 6$ . Sample point distribution of  $P_N$  is illustrated in Fig. 4.

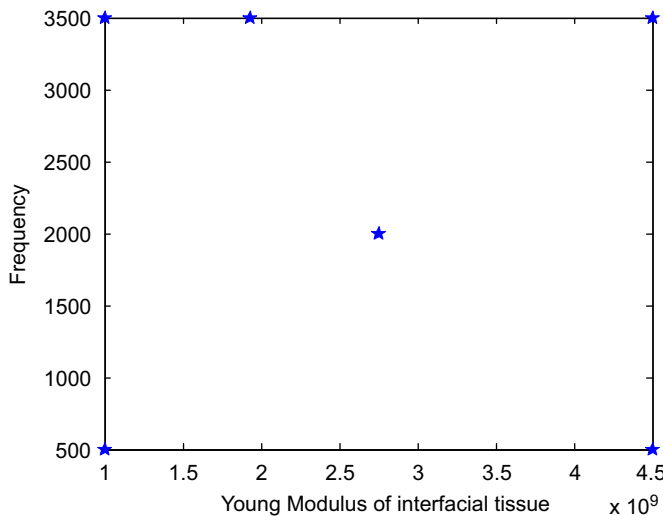


Fig. 4. Distribution of reduced-basis sample set for RBM model obtained by the adaptive sampling procedure using the greedy algorithm.

Another parameter set  $S_{test}$  including a total of  $n_{test} = 500$  samples is randomly created. For two parameters:  $\mu_{test-1} = (2.05 \times 10^9 \text{ Pa}, 2500 \text{ Hz})$  and  $\mu_{test-2} = (1.7 \times 10^9 \text{ Pa}, 1800 \text{ Hz})$ , asymptotic errors and exact errors are evaluated and compared as a function of  $N$  as shown in Figs. 5 and 6. The averaged asymptotic and averaged exact errors over the entire  $S_{test}$  are also compared and plotted in Fig. 7. The numerical results suggest that our asymptotic error is in good agreements with the exact error, and the convergence rate of the reduced-basis method is very fast for an  $N \ll \mathfrak{N}$ .

Additionally, the maximum error difference  $e = |\Delta_{N,M}^s(\mu_{max}) - \Delta_{N,exact}^s(\mu_{max})|$ , and the affectivity  $\eta = (\Delta_{N,M}^s(\mu_{max}) / \Delta_{N,exact}^s(\mu_{max}))$  at  $\mu_{max} \in S_{test}$  are computed at  $N_{max} = 6$ . We obtain  $e = 3.8817 \times 10^{-10}$  and  $\eta = 0.999977$  which is indeed very close to one. These results confirm that the asymptotic error is very effective, easy to implement, and it has the property of close-to-unity affectivity.

Computation time for a RBM forward solver ( $t_{RBM(online)}$ ), CPU-time for a FEM forward solver ( $t_{FEM}$ ), and the CPU-time saving factor  $\alpha = t_{FEM} / t_{RBM(online)}$  are also listed in Table 2. It is

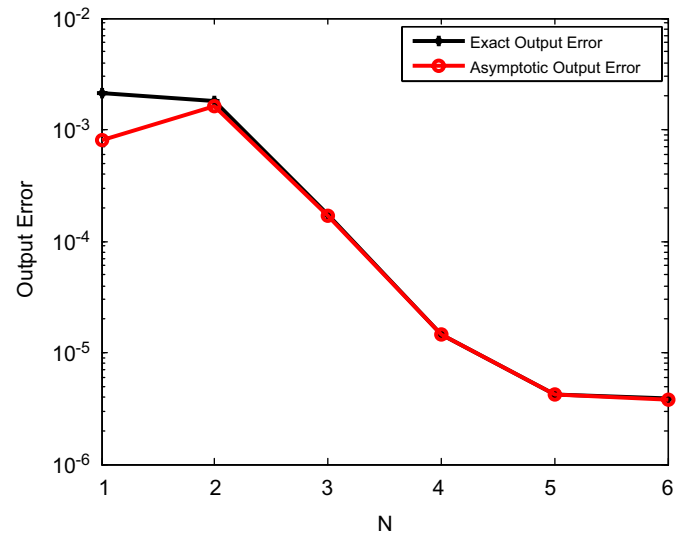


Fig. 5. Comparison between the asymptotic error and the exact output error for  $\mu_{test-1} = (2.05 \times 10^9 \text{ Pa}, 2500 \text{ Hz})$ .

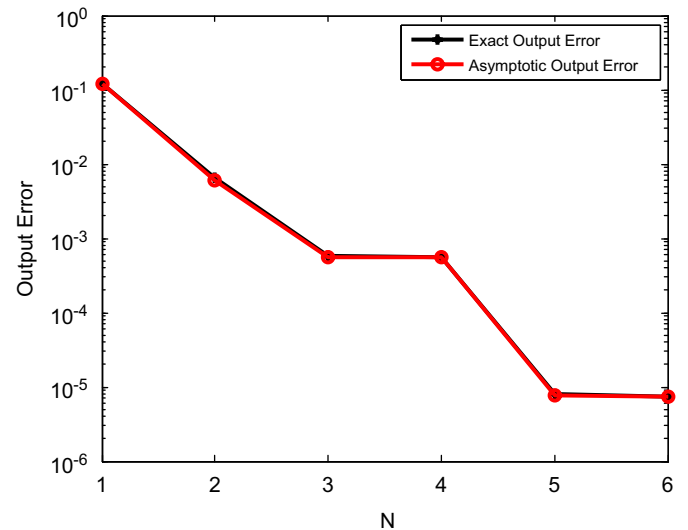


Fig. 6. Comparison between the asymptotic error and the exact output error for  $\mu_{test-2} = (1.7 \times 10^9 \text{ Pa}, 1800 \text{ Hz})$ .

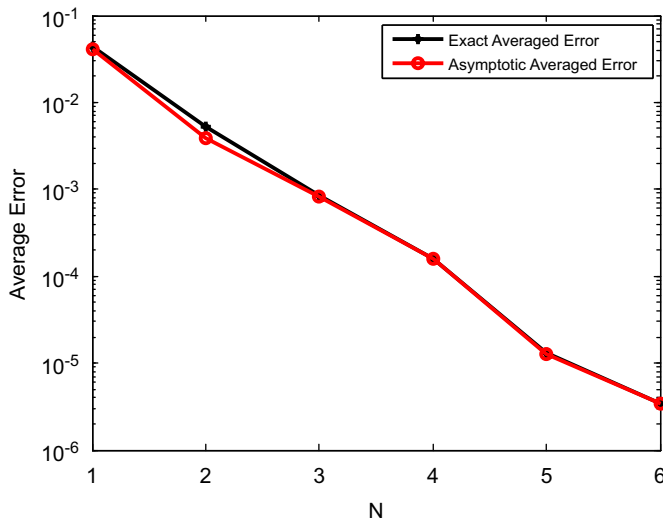


Fig. 7. Comparison between the averaged asymptotic error and averaged exact error.

Table 2

Comparison of CPU-time for a FEM and a RBM forward analysis.

N	$t_{FEM}$	$t_{RBM(online)}$	$\alpha = t_{FEM}/t_{RBM(online)}$
6	53.3614 (s)	$8.0493 \times 10^{-5}$ (s)	$6.6293 \times 10^5$

Note: Test on a PC of Intel®, Pentium(R) D, CPU 3.4 GHz, 2GB Ram.

recognized that the RBM is very efficient for solving forward problems. From the numerical results, it is likely that the reliability and efficiency of our RBM model is promising. Our RBM model is now ready to be utilized as an efficient forward solver in inverse analysis.

### 3. Inverse procedure

We next establish an inverse procedure using our RBM model together with a neural network model to identify rapidly the elastic modulus  $E$  of interfacial tissue in our implanted bone structure.

#### 3.1. Briefing on neural network

A NN model is built by using an artificial set of nodes called neurons arranged by several layers including input layer, one or more hidden layers and output layer (see, e.g., Liu and Han, 2003). The diagram of a NN model with two hidden layers is shown in Fig. 8, in which the lines between nodes indicate the information flows from input-layer nodes to hidden-layer nodes and from hidden-layer nodes to output-layer nodes.

In a NN, inputs are selected based on the knowledge of sensitivity analysis, and fed into the input layer. Input-layer neurons send their inputs to hidden-layer nodes without any modification. Arriving at hidden-layer neurons, the values from input-layer neurons are modified as shown in Fig. 9 by multiplying interconnection weights. Before leaving the neurons, the resulting weighted values are summed together producing a single-combined value which is then fed into a nonlinear activation function called 'sigmoid function' and an output is produced. Outputs from the hidden-layer neurons are then passed

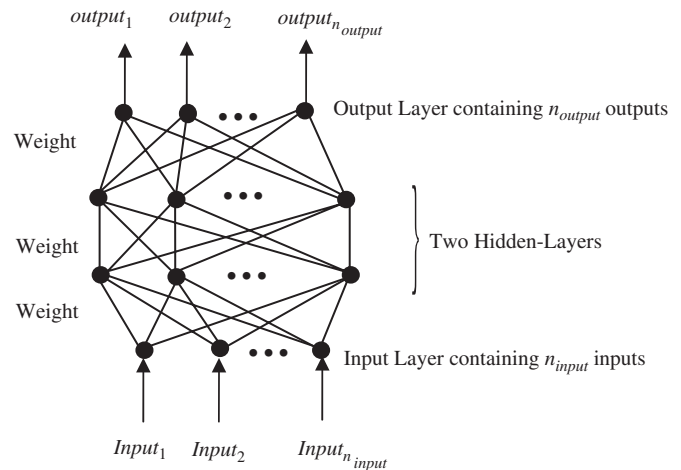


Fig. 8. A NN model with two-hidden-layer,  $n_{input}$  inputs and  $n_{output}$  outputs.

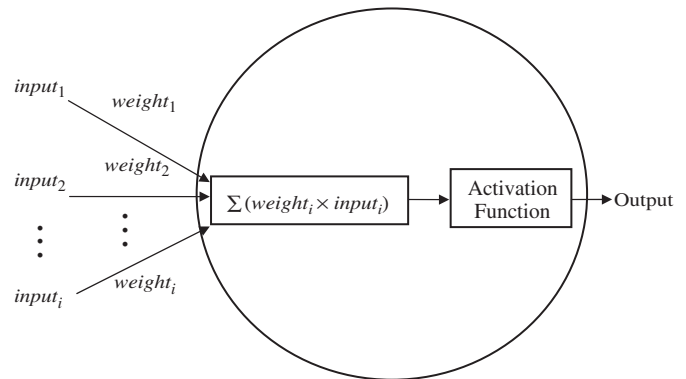


Fig. 9. A typical neuron in hidden layers and output layer of the neural network.

on to output-layer neurons. Again, output-layer neurons modify these values as the same way in the hidden layers, and produce reasonable outputs of the NN. Note that the NN model is trained with a modified back-propagation learning algorithm (see, e.g., Liu and Han, 2003) in terms of determining and adjusting inter-connection weights. In this work, a NN model is built including an input layer, two hidden layers and an output layer. The neuron numbers of the four layers are given as 4, 16, 8 and 1, respectively.

#### 3.2. Numerical analysis

##### 3.2.1. Comparison of RBM outputs and experimental measurements

We should examine our RBM results and experimental results before the application of neural network. Using the RFA device, experiments are made and measurements are recorded when the self-curing resin is completely solidified. Measurements are then compared with our RBM results and the results of the full FEM model in term of frequency response within the frequency range of [800,3500] Hz. As shown in Fig. 10, the normalized results obtained using our RBM model are in very good agreements with that of the experimental measurements.

##### 3.2.2. Inputs of NN model

In a NN, it is necessary to determine inputs which are significantly influenced Young's modulus  $E$  of interfacial tissues. Hence, effects of displacement responses, at the position where

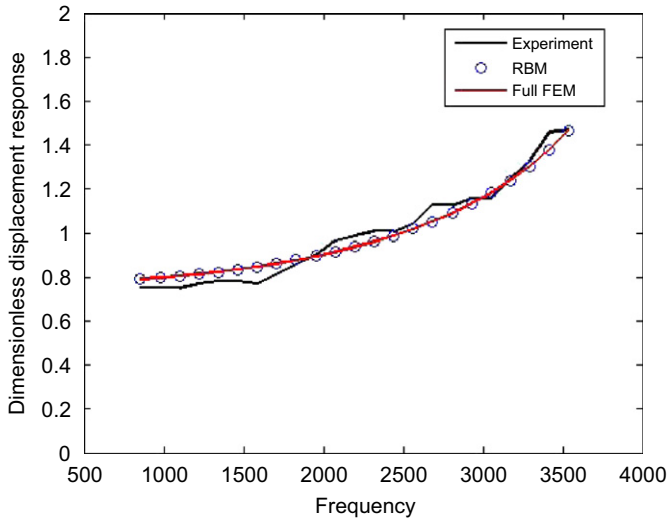


Fig. 10. Comparison of experimental, full FEM and RBM solutions.

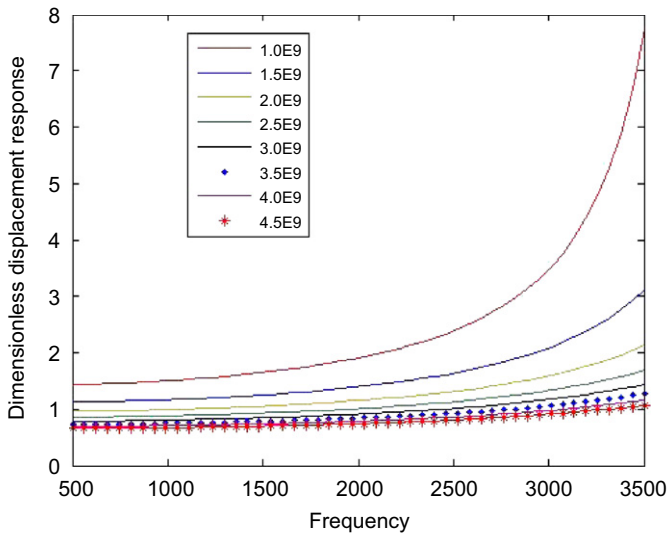


Fig. 11. Effect of Young's modulus of interface resin  $E$  on displacement responses.

harmonic force is applied (see Fig. 3), are analyzed in  $\mathcal{D} = [1.0 \times 10^9, 4.5 \times 10^9] \text{ Pa} \times [500, 3500] \text{ Hz} \subset \mathbb{R}^{P=2}$  over which our RBM model is constructed. Effects on displacement responses with respect to  $E$  of interfacial tissues and  $\omega$  are plotted in Fig. 11. It is shown that the response is quite sensitive to  $E$  and very sensitive to  $\omega$  within the range of  $\omega = [2500 \text{ Hz}, 3500 \text{ Hz}]$ . Hence, displacement responses at four  $\omega$ :  $\omega_1 = 3051.3 \text{ Hz}$ ,  $\omega_2 = 3173.3 \text{ Hz}$ ,  $\omega_3 = 3295.4 \text{ Hz}$ , and  $\omega_4 = 3417.5 \text{ Hz}$  are selected as inputs of our NN mode. The NN model is then trained using a set of training samples and their corresponding displacement responses at  $\omega_i$ ,  $i = 1, \dots, 4$ , which are generated by our RBM model.

### 3.2.3. Training of NN model

A set of training samples which covers all the possible values of  $E$  should be firstly defined to construct a reliable NN model. The orthogonal array (OA) method (e.g., Besterfield et al., 1995) has been adopted to generate a training sample set. In this work, the search range within  $\pm 50\%$  off the “true” parameter  $E_{true}$  is used, and ten training samples of  $E$  are determined by dividing evenly within the search range, excluding  $E_{true}$ . Each training sample is

Table 3

Determination of Young's modulus of resin using the RBM–NN and experimental measurements.

Original Young's Modulus	$E_{actual} = 2.94 \times 10^9 \text{ (Pa)}$	
Search range	$\pm 50\%$	
Neural network	Identified results $2.8639 \times 10^9 \text{ (Pa)}$	Error –2.5884%

input into our RBM model in order to generate corresponding displacement responses. The NN model is then trained using the training sample set and corresponding displacement responses obtained using the RBM model. The trained NN is then used to nondestructively identify  $E_{true}$  by feeding “measured” displacement responses.

### 3.2.4. Simulated and experimental measurements

To verify our RBM–NN procedure, both experimental “measured” displacements and simulated “measured” displacements are used as input to the NN model. For simulated measurements, an “artificial” Gauss noise with mean 0 and deviation  $d_{std}$  is added to our RBM displacement responses (see, e.g., Han et al., 2003), where

$$d_{std} = c \times \left[ \frac{1}{n_{input}} \left( \sum_{i=1}^{n_{input}} \tilde{s}(E_{true}, \omega_i) \right)^2 \right]^{0.5}, \quad (11)$$

where  $\tilde{s}(E_{true}, \omega_i)$ ,  $i = 1, \dots, 4$ , are the FEM displacement responses,  $n_{input}$  is the number of inputs for the NN model, and  $c$  is the value of noise contamination lever. In this work,  $c$  is set at 0.05. It means that simulated measurements are contaminated with 5% noise to use in inverse analyses.

In the NN, the inputs, the training data, and outputs are usually normalized in the range 0.1–0.9. The normalization is performed in the following references (Deng et al., 2008c; Liu and Han, 2003).

### 3.2.5. Applications of NN and results

To examine the stability of the RBM–NN approach, inverse analyses are now performed using the trained NN model. In-vitro experimental measurements at the actual Young's modulus  $E_{actual}$  and  $\omega_i$ ,  $i = 1, \dots, 4$  are input into the NN model, and the required output is inversely identified. The identified  $E$  of interfacial tissue is given in Table 3. Two additional cases of inverse analyses are also conducted in which the noise-free and 5% noise-contaminated-simulated measurements are used. Tables 4 and 5 give estimated elastic moduli for two “true” elastic moduli of  $E_{true-1}$  and  $E_{true-2}$ . The RBM–NN estimate results with maximum errors of less than 1% for noise-free case, and less than 5% for both 5% noise-contaminated cases and in-vitro experiment case. The results interpret that our inverse procedure is very stable and reliable within the search range of  $\pm 50\%$  off  $E_{true}$ . This search range is sufficient in practical applications.

To validate the efficiency of the RBM–NN approach, total forward solver calls for a RBM–NN inverse analysis are also given in Table 6; total CPU time is then recorded and provided in Table 7. It is found that CPU time for a NN model using the RBM solver is significantly faster than that of using the FEM solver. Therefore, the proposed RBM–NN approach drastically cuts down computational time and cost.

**Table 4**  
Determination of Young's modulus of resin using the RBM–NN and simulated measurements with 0% and 5% noise contamination for  $E_{true-1}$ .

Original Young's modulus	$E_{true-1} = 1.5 \times 10^9$ (Pa)			
Search range	$\pm 50\%$			
Neural network	Noise free		Noise added (5%)	
	Identified results $1.4910 \times 10^9$ (Pa)	Error 0.6%	Identified results $1.4252 \times 10^9$ (Pa)	Error 4.9867%

**Table 5**  
Determination of Young's modulus of resin using the RBM–NN and simulated measurements with 0% and 5% noise contamination for  $E_{true-2}$ .

Original Young's modulus	$E_{true-2} = 2.0 \times 10^9$ (Pa)			
Search range	$\pm 50\%$			
Neural network	Noise free		Noise added (5%)	
	Identified results $1.9960 \times 10^9$ (Pa)	Error 0.2%	Identified Results $2.0988 \times 10^9$ (Pa)	Error –4.94%

**Table 6**  
Total number of forward analyses required in a RBM–NN inverse analysis.

Number of training samples	Number of RBM calls in each training sample	Total RBM calls in a NN model
10	4	$m = 40$

**Table 7**  
Comparison of computational time for a NN model using FEM and RBM as forward solvers.

Total RBM calls for a NN model	CPU time for each forward solver		Total computational time	
$m = 40$	$t_{FEM}$	53.3614 (s)	$m \times t_{FEM}$	35.5743 (min)
	$t_{RBM(online)}$	$8.0493 \times 10^{-5}$ (s)	$m \times t_{RBM(online)}$	$3.2197 \times 10^{-3}$ (s)

#### 4. Conclusion

In this paper, a rapid inverse procedure (RBM–NN) is established consisting of four main stages: constructing a fast RBM forward solver, choosing inputs for the NN model, training the NN model and determining the elastic modulus. The elastic moduli of interfacial tissues in the dental implant–bone structure are successfully identified by feeding experimental measurements and/or simulated measurements through the trained NN model. The inversely identified results of the RBM–NN procedure are very accurate for all the experiment case, noise-free cases and noise-contaminated cases. The results of our example support to conclude that the computational efficiency is increased due to the use of the RBM, and inversely identified results are stable and reliable due to a novel information processing feature of the NN techniques, which is able to model non-linear relation between structural parameter and non-static responses of complex dental implant structures.

#### Conflict of interest statement

All authors would like to thank the “Agency for Science, Technology and Research (A\*STAR), Singapore” for the financial support for this work that could have influenced its outcome.

#### References

- Besterfield, D.H., Besterfield-Michna, C., Besterfield, G.H., Besterfield-Sacre, M., 1995. Total Quality Management. Prentice-Hall, Inc., Englewood Cliffs.
- Brånemark, P.I., Zarb, G.A., Albrektsson, T. (Eds.), 1985. Tissue-Integrated Protheses: Osseointegration in Clinical Dentistry. Quintessence Publishing Co. Inc., Chicago.
- Brunski, J.B., 1992. Biomechanical factors affecting the bone–dental implant interface. Clin. Mater. 10, 153–201.
- Cowin, S.C., 1986. Wolff's law of trabecular architecture at remodeling equilibrium. J. Biomech. Eng. 108, 83–88.
- Cowin, S.C., 2001. Bone Mechanics Handbook. CRC Press, Boca Raton, FL.
- Deng, B., Han, X., Liu, G.R., Tan, K.B.C., 2004. Prediction of elastic properties of the maxillary bone. Proceeding of WCCM VI in conjunction with APCOM'04, Computational Mechanics.
- Deng, B., Tan, K.B.C., Liu, G.R., 2008a. Influence of osseointegration degree and pattern on resonance frequency in the assessment of dental implant stability using finite element analysis, Int. J. Oral Maxillofac. Implants, submitted for publication.
- Deng, B., Tan, K.B.C., Liu, G.R., Geng, J.P., Yan, W.Q., 2008b. A new numerical approach for evaluation of dental implant stability using electromagnetic impulse. Int. Chin. J. Dent. 8, 1–9.
- Deng, B., Tan, K.B.C., Liu, G.R., Zaw, K., 2008c. Inverse identification of anisotropic elastic constants of dental implant–bone interfacial tissue using neural network and FEA model, Inverse Probl. Sci. Eng., 2008c, revised.
- Friberg, B., Jemt, T., Lekholm, U., 1991. Early failures in 4641 consecutively placed Brånemark dental implants: a study from stage 1 surgery to the connection of completed protheses. Int. J. Oral Maxillofac. Implants 6, 142–146.
- Geng, J.P., Tan, K.B.C., Liu, G.R., 2001. Application of finite element analysis in implant dentistry: a review of the literature. J. Prosthet. Dent. 85, 585–598.

- Grepl, M.A., Patera, A.T., 2005. A posteriori error bounds for reduced-basis approximations for parameterized parabolic partial differential equations. *ESAIM: Math. Model. Numer. Anal. (M2AN)* 39, 157–181.
- Grepl, M.A., Nguyen, N.C., Veroy, K., Patera, A.T., Liu, G.R., 2007. Certified rapid solution of partial differential equations for real-time parameter estimation and optimization. *Real-Time PDE-Constrained Optimization*. SIAM Computational Science and Engineering Book Series, pp. 197–212.
- Han, X., Liu, G.R., 2003. Computational inverse techniques for material characterization of functionally graded materials. *AIAA J.* 41, 288–295.
- Han, X., Xu, D., Yap, F.F., Liu, G.R., 2002. On determination of the material constants of laminated cylindrical shells based on an inverse optimal approach. *Inverse Probl. Eng.* 10, 309–322.
- Han, X., Xu, D.L., Liu, G.R., 2003. A computational inverse technique for material characterization of a functionally graded cylinder using a progressive neural network. *Neurocomputing* 51, 341–360.
- Huber, N., Tsakmakis, C., 1999. Determination of constitutive properties from spherical indentation data using neural networks. Part I: the case of pure kinematic hardening in plasticity laws. *J. Mech. Phys. Solids* 47, 1569–1588.
- Huynh, D.B.P., Patera, A.T., 2006. Reduced-basis approximation and a posteriori error estimation for stress intensity factor. *Int. J. Numer. Methods Eng.* 00, 1–6.
- Liu, G.R., 2008. A generalized gradient smoothing technique and the smoothed bilinear form for Galerkin formulation of a wide class of computational methods. *Int. J. Comput. Methods* 5, 199–236.
- Liu, G.R., Han, X., 2003. *Computational Inverse Techniques in Nondestructive Evaluation*. CRC Press, Boca Raton, FL.
- Liu, G.R., Han, X., Lam, K.Y., 2001a. Material characterization of FGM plates using elastic waves and an inverse procedure. *J. Comput. Mater.* 35, 954–971.
- Liu, G.R., Han, X., Xu, Y.G., Lam, K.Y., 2001b. Material characterization of functionally graded material by means of elastic waves and a progressive-learning neural network. *Comput. Sci. Technol.* 61, 1401–1411.
- Liu, G.R., Han, X., Lam, K.Y., 2002a. A combined genetic algorithm and nonlinear least square method for material characterization using elastic waves. *Comput. Methods Appl. Mech. Eng.* 191, 1909–1921.
- Liu, G.R., Han, X., Ohyoshi, T., 2002b. Computational inverse techniques for material characterization using dynamic response. *Int. J. Soc. Mater. Eng. Resour.* 10, 26–33.
- Liu, G.R., Khin, Zaw, Wang, Y.Y., Deng, B., 2008a. A novel reduced-basis method with upper and lower bounds for real-time computation of linear elasticity problems. *Comput. Methods Appl. Mech. Eng.* 198, 269–279.
- Liu, G.R., Khin, Zaw, Wang, Y.Y., 2008b. Rapid inverse parameter estimation using reduced-basis approximation with asymptotic error estimation. *Comput. Methods Appl. Mech. Eng.* 197, 3898–3910.
- Liu, G.R., Lee, J.H., Patera, A.T., Yang, Z.L., Lam, K.Y., 2005. Inverse identification of thermal parameters using reduced-basis method. *Comput. Methods Appl. Mech. Eng.* 194, 3090–3107.
- Meredith, N., Alleyne, D., Cawley, P., 1996. Quantitative determination of the stability of the implant–tissue interface using resonance frequency analysis. *Clin. Oral Implants Res.* 7, 261–267.
- Nguyen, N.C., 2005. Reduced-basis approximation and a posteriori error bounds for non-affine and non-linear partial differential equations: application to inverse analysis. Ph.D. Thesis, Singapore-MIT alliance.
- Patera, A.T., Rønquist, E.M., 2007. Reduced basis approximation and a posteriori error estimation for a Boltzmann model. *Comput. Methods Appl. Mech. Eng.* 196, 2925–2942.
- Prud'homme, C., Rovas, D.V., Veroy, K., Machiels, L., Maday, Y., Patera, A.T., Turinici, G., 2002. Reliable real-time solution of parameterized partial differential equations: reduced-basis output bound methods. *J. Fluid Eng.* 124, 70–80.
- Rozza, G., Veroy, K., 2007. On the stability of the reduced basis method for stokes equations in parameterized domains. *Comput. Methods Appl. Mech. Eng.* 196, 1244–1260.
- Sennerby, L., Persson, L.G., Berglundh, T., Wennerberg, A., Lindhe, J., 2005. Implant stability during initiation and resolution of experimental periimplantitis: an experimental study in the dog. *Clin. Implant Dent. Relat. Res.* 7, 136–140.
- Sribar, R., 1994. Solutions of inverse problems in elastic wave propagation with artificial neural networks. Dissertation, Cornell University, Ithaca, NY.
- Sumpter, B.G., Noid, D.W., 1996. On the design, analysis, and characterization of materials using computational neural networks. *Annu. Rev. Mater. Sci.* 26, 223–277.
- Veroy, K., Patera, A.T., 2005. Certified real-time solution of the parameterized steady incompressible Navier–Stokes equations: rigorous reduced-basis a posteriori error bounds. *Int. J. Numer. Methods Fluid* 47, 773–788.